TU/e EINDHOVEN UNIVERSITY OF TECHNOLOGY

Adjoint-based design optimization of a Kenics static mixer

Citation for published version (APA):
Morales Ubal, C., Beishuizen, N., Kusch, L., & van Oijen, J. (2024). Adjoint-based design optimization of a Kenics static mixer. *Results in Engineering*, *21*, Article 101856. https://doi.org/10.1016/j.rineng.2024.101856

Document license:
CC BY-NC-ND

DOI:
10.1016/j.rineng.2024.101856

Document status and date:
Published: 01/03/2024

Document Version:
Publisher's PDF, also known as Version of Record (includes final page, issue and volume numbers)

Please check the document version of this publication:

• A submitted manuscript is the version of the article upon submission and before peer-review. There can be important differences between the submitted version and the official published version of record. People interested in the research are advised to contact the author for the final version of the publication, or visit the DOI to the publisher's website.
• The final author version and the galley proof are versions of the publication after peer review.
• The final published version features the final layout of the paper including the volume, issue and page numbers.

Link to publication

General rights
Copyright and moral rights for the publications made accessible in the public portal are retained by the authors and/or other copyright owners and it is a condition of accessing publications that users recognise and abide by the legal requirements associated with these rights.

• Users may download and print one copy of any publication from the public portal for the purpose of private study or research.
• You may not further distribute the material or use it for any profit-making activity or commercial gain
• You may freely distribute the URL identifying the publication in the public portal.

If the publication is distributed under the terms of Article 25fa of the Dutch Copyright Act, indicated by the "Taverne" license above, please follow below link for the End User Agreement:

www.tue.nl/taverne

Take down policy
If you believe that this document breaches copyright please contact us at:

openaccess@tue.nl

providing details and we will investigate your claim.

Download date: 23. Nov. 2026

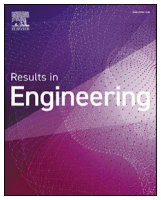
Results in Engineering 21 (2024) 101856



Contents lists available at ScienceDirect

Results in Engineering

journal homepage: www.sciencedirect.com/journal/results-in-engineering



Research paper

Adjoint-based design optimization of a Kenics static mixer

Cristopher Morales Ubal [a,*], Nijso Beishuizen [a,c], Lisa Kusch [b], Jeroen van Oijen [a]

[a] Eindhoven University of Technology, Power & Flow Group, Eindhoven, the Netherlands
[b] University of Kaiserlautern-Landau, Kaiserslautern, Germany
[c] Bosch Thermotechnology, Deventer, the Netherlands

ARTICLE INFO

Keywords:
Kenics static mixer
Computational fluid dynamics
Adjoint design optimization
Mixing gas model
Turbulent flow
Laminar flow

ABSTRACT

Mixing processes are important in many applications like food processing or in chemical reactors. Achieving homogeneous mixtures over short distances with a small pressure drop is a challenge. Kenics static mixers usually provide a good balance between pressure drop and mixing quality. Nevertheless, little attention has been paid to the use of this mixing device in mixing gases, and consequently relatively large pressure drops are obtained. In this paper, the discrete adjoint method is used to obtain optimized Kenics static mixer designs with a negligible increase in pressure drop. First, a framework of a composition-dependent model based on the ideal gas mixing laws for thermochemical properties is implemented and coupled to the existing discrete adjoint solver within SU2, which is an open-source software suite for multiphysics simulations and design optimization. Subsequently, in order to identify the key geometrical parameters that affect the pressure drop in the mixer, numerical simulations are performed for different aspect ratios, blade thicknesses, and Reynolds numbers. These results are compared with available simulations and correlations reported in the literature, showing good agreement. These simulations indicate that reducing the aspect ratio and increasing the blade thickness enhance the mixing process in the mixing units. However, a substantial increase in pressure drop is observed. The results of the parameter study are used as a starting point to optimize the blade designs inside the Kenics static mixer using a discrete adjoint approach. The objective is to minimize the variance of the mass fraction at the outlet, which is a measure of mixture homogeneity, without substantially increasing the pressure drop along the mixing device. The results indicate that an optimized design can be obtained with a negligible increase in pressure drop, highlighting the capabilities of the discrete adjoint design approach as an optimization tool for mixing devices.

1. Introduction

Binary mixing of fluids is an important problem in many industrial applications such as food processing or combustion. This is the case for combustion technologies where there is increasing demand for high fuel efficiency and low pollutant emissions. In premixed combustion for instance, air and fuel are mixed before entering the combustion chamber. For this purpose, a mixer device is used in order to supply a homogeneous mixture of fuel and air. Having non-homogeneous fuel/air ratio can result in unstable operation and trigger excessive emissions, which might cause them to exceed environmental regulations [1]. In modern industrial processes, mixing is mainly done in static mixer devices [2], which consist of a series of identical elements or units organized in a structured configuration [2]. These elements are added to pipes, reactors, and other equipment in order to promote the mixing between two or more fluids through redistribution, splitting, rotation, and remixing of the fluids [3]. Among the different types of static mixers widely reported in the literature [3,4], the Kenics static mixer has shown a good capability for enhancing the mixing process [5–8]. This is due to its geometry, which consists of a tube with a sequence of thin blades twisted 180° (mixer element), where each blade starts perpendicular with respect to the previous blade (see Fig. 1).

Some experimental and numerical research to study and understand the flow and mixing process along Kenics static mixers can be found in the literature. Hobbs et al. [5] performed 3D numerical simulations for laminar flows (with Reynolds numbers Re < 1000) obtaining good

* Corresponding author.
E-mail address: c.l.morales.ubal@tue.nl (C. Morales Ubal).

https://doi.org/10.1016/j.rineng.2024.101856
Received 15 August 2023; Received in revised form 26 January 2024; Accepted 28 January 2024
Available online 5 February 2024
2590-1230/© 2024 Published by Elsevier B.V. This is an open access article under the CC BY-NC-ND license (http://creativecommons.org/licenses/by-nc-nd/4.0/).

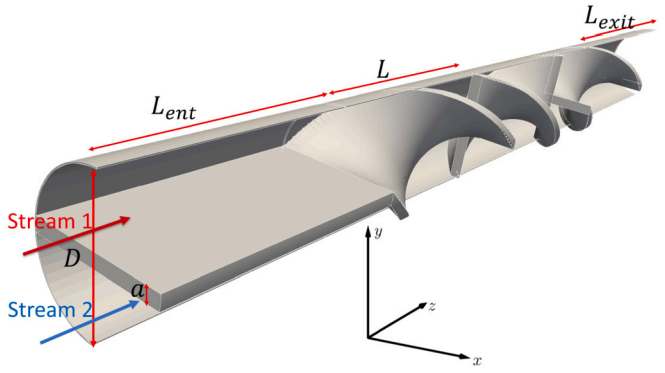


Fig. 1. Schematic representation of a Kenics static mixer with an entrance part, 3 mixer elements, and an exit part.

agreement with experimental correlations for pressure drop available in the literature. Kumar et al. [9] extended the numerical simulations to a wider range of Reynold numbers ($1 < \mathrm{Re} < 25000$). They obtained a new correlation for pressure drop that was obtained from experiments and numerical simulations. Both studies [5,9] highlighted the increase of pressure drop with increasing Reynolds number. Joshi et al. [8] conducted experiments where the effect of the aspect ratio of a mixing element ($AR = L/D$), which is the ratio between the element length (L) and the diameter of the Kenics static mixer (D), was included, obtaining a correlation for pressure drop for laminar flows. Following the aforementioned work, Song et al. [7] formulated a correlation for pressure drop based on numerical simulations for a wide range of Re including the AR. Recently, Jiang et al. [10] studied the effect of aspect ratio on the mixing performance of a Kenics static mixer with different numbers of mixing elements. It was found that a lower aspect ratio caused a reduction in the mixing time. Nevertheless, they also observed that in order to increase the mixing performance, more elements must be added, leading to an increase in the pressure drop. Furthermore, Jiang et al. [11] extended their research by investigating the effect of the blade thickness (a) on the pressure drop. They found that the blade thickness has a direct impact on the pressure drop. A new pressure drop correlation was deduced from the numerical simulations that includes the dependence on Re, AR and a.

Although considerable research has been devoted to understanding the mixing mechanism of liquids in the Kenics static mixers, less attention has been paid to using them as a mixing device for (binary) gases. Furthermore, the mixing efficiency was mainly increased by changing the AR, a or adding more mixing units, which caused a large increase in pressure drop. A different strategy to enhance the mixing processes without a substantial increase on the pressure drop has not been reported. Therefore, in the present work an automatic discrete adjoint-based design approach is used to obtain optimized Kenics static mixers. This approach is a gradient-based design optimization that allows for single and multipoint optimization of a objective functions at a computational cost that is roughly equal to an additional CFD simulation [12,13]. In order to achieve this, a general workflow is implemented, which consists of the implementation of a composition-dependent model for multi-species flows based on the mixing law for ideal gases. This method is coupled to the discrete adjoint solver implemented in the multiphysics CFD and optimization suite SU2 [12–15]. Subsequently, in order to identify the key parameters of the mixing device under study, CFD simulations are performed for different AR, a and Re, where pressure drop and mixing effectiveness are investigated. Finally, taking into account the previous CFD simulations, the discrete adjoint-based design approach is applied to obtain optimized Kenics static mixer designs. The results obtained in this work provide new insights on applying an efficient optimization tool for a well-known mixing device.

2. Computational model

2.1. Governing equations

The flows (simulations) in this paper are assumed to be three dimensional, steady, isothermal and incompressible. The CFD solution is obtained by solving the partial differential Navier-Stokes (N-S) equations which correspond to transport equations for the mass (1), momentum (2) and species mass fraction (3) for the conservative variables $\mathbf{U} = \left[\rho, \rho\mathbf{v}, \rho Y_i\right]$, and are given by:

$$\frac{\partial \rho}{\partial t} + \nabla \cdot (\rho \mathbf{v}) = 0\,, \tag{1}$$

$$\frac{\partial \rho \mathbf{v}}{\partial t} + \nabla \cdot (\rho \mathbf{v}\mathbf{v}) + \nabla p - \nabla \cdot \boldsymbol{\tau} = 0\,, \tag{2}$$

$$\frac{\partial \rho Y_i}{\partial t} + \nabla \cdot \left(\rho Y_i \mathbf{v}\right) - \nabla \cdot \left(\rho D_i \nabla Y_i\right) = 0\,,\ \forall i = 1, \ldots, N \tag{3}$$

where $\mathbf{v}$ is the velocity field, ρ is the density, p is the pressure, D_i is the mass diffusivity of the species i into the mixture, and Y_i is the mass fraction of species i. As the N species equations in (3) together with the continuity equation (1) are over-determined, only $N-1$ species equations are solved from (3). The last species mass fraction is obtained from:

$$Y_N = 1 - \sum_{i=1}^{N-1} Y_i\,. \tag{4}$$

Moreover, the compressible form for the shear stress tensor $\boldsymbol{\tau}$ is used and given as follows:

$$\boldsymbol{\tau} = \mu \left(\nabla \mathbf{v} + (\nabla \mathbf{v})^T - \frac{2}{3} (\nabla \cdot \mathbf{v}) \mathbf{I} \right)\,, \tag{5}$$

where $\mathbf{I}$ is the unit tensor. How the fluid properties ρ, μ and D_i are computed based on the fluid composition will be explained in the next section.

For modelling turbulence we solve the Reynolds-Averaged Navier Stokes equations (RANS) considering the Boussinesq hypothesis [16], where the effect of turbulence is modelled as an increase in viscosity. Therefore, the viscosity becomes an effective viscosity given by:

$$\mu_{\mathrm{eff}} = \mu + \mu_t\,, \tag{6}$$

where μ and μ_t are the laminar and turbulent viscosities of the gas mixture, respectively. The same approach is adopted for the mass diffusivity which is computed by:

$$D_{i,\mathrm{eff}} = D_i + \frac{\mu_t}{\mathrm{Sc_t}}\,, \tag{7}$$

where $\mathrm{Sc_t}$ is the turbulent Schmidt number taken as 0.7 [17].

For computing μ_t, the Shear Stress Transport ($k-\omega$ SST) model of Menter [18] is used given its well-extensive validation through three-dimensional incompressible steady flows, in particular for Kenics static mixer simulations [9–11]. In this approach, two additional transport equations are solved for the turbulent kinetic energy k, and turbulent dissipation rate ω, which are given below:

$$\frac{\partial \rho k}{\partial t} + \nabla \cdot (\rho k \mathbf{v}) = \nabla \cdot \left[\left(\mu + \sigma_k \mu_t\right) \nabla k\right] + P_k - \beta^* \rho \omega k\,, \tag{8}$$

$$\frac{\partial \rho \omega}{\partial t} + \nabla \cdot (\rho \omega \mathbf{v}) = \nabla \cdot \left[\left(\mu + \sigma_\omega \mu_t\right) \nabla k\right] + \frac{\gamma}{\nu_t} P_k - \beta^* \rho \omega^2 + 2\left(1 - F_1\right) \frac{\rho \sigma_{\omega,2}}{\omega} \nabla k \cdot \nabla \omega\,, \tag{9}$$

where σ_k, σ_ω, β^*, γ and $\sigma_{\omega,2}$ are closure coefficient and auxiliary relations, F_1 and F_2 are blending coefficients, and P_k is the production term. More details about these terms are given in [18].

Although the N-S equations above are written in the conservative form, for incompressible flows the primitive variables $V = \left[p, \mathbf{v}, Y_i, k, \omega\right]$ are solved for. Moreover, the discretization of the set of equations (1),

(2), (3), (8) and (9) forms the system which will be referred to as $R(V) = 0$ when the adjoint method will be explained in section 2.4. Finally, the N-S equations are solved using a preconditioning approach for low-Mach number incompressible flows, which are discretized using a finite volume method on a vertex-based median-dual grid [14].

2.2. Mixing model

The composition-dependent model presented in this paper is based on the mixing laws for ideal gases. First, the mean molecular weight (W) is determined as follows [17]:

$$W = \left[\sum_{i=1}^{N} \frac{Y_i}{W_i}\right]^{-1} , \tag{10}$$

where W_i is the molecular mass of species i.

Adopting the low-Mach number approximation [19], the thermodynamic pressure can be decoupled from the governing equations (2) and can be set constant. Then, using (10), the density is given by [17]:

$$\rho = \frac{p_{\text{op}}}{RT/W} , \tag{11}$$

where p_{op} is the thermodynamic (or operating) pressure, set as 101325 Pa, T is the temperature and R is the universal gas constant which value is 8.314 J / (mol· K).

The specific heat capacity at constant pressure and volume are computed as a mass fraction average of the individual species heat capacities [17],

$$C_p = \sum_{i=1}^{N} Y_i C_{p,i} , \tag{12}$$

$$C_v = C_p - \frac{R}{W} , \tag{13}$$

where $C_{p,i}$ is the mass specific heat capacity at constant pressure of species i.

Wilke's method based on kinetic theory is used to compute the laminar viscosity μ of a gas mixture:

$$\mu = \sum_{i=1}^{N} \frac{X_i \mu_i}{\sum_{j=1}^{N} X_j \phi_{ij}} , \tag{14}$$

where μ_i are the laminar viscosities of species i and ϕ_{ij} are binary coefficients computed by:

$$\phi_{ij} = \frac{\left[1 + \left(\frac{\mu_i}{\mu_j}\right)^{1/2} \left(\frac{W_j}{W_i}\right)^{1/4}\right]^2}{\left[8\left(1 + \frac{W_i}{W_j}\right)\right]^{1/2}} , \tag{15}$$

and, X_i is the mole fraction of species i given by:

$$X_i = \frac{W}{W_i} Y_i . \tag{16}$$

Similarly, following Wilke's approach, the thermal conductivity for a gas mixture is computed as follows [20]:

$$\kappa = \sum_{i=1}^{N} \frac{X_i \kappa_i}{\sum_{j=1}^{N} X_j \phi_{ij}} , \tag{17}$$

where, κ_i is the thermal conductivity of species i and ϕ_{ij} is computed by (15). Finally, the mass diffusivity coefficient, D_i, which measures the fluid transport process due to molecular motion is based on the constant Lewis number assumption. The Lewis number, Le_i, compares the heat diffusivity with respect to mass diffusivity [17],

$$\text{Le}_i = \frac{\text{Sc}_i}{\text{Pr}} , \tag{18}$$

where Sc_i and Pr are the Schmidt and Prandtl number, respectively. As $\text{Pr} = \mu \cdot C_p/\kappa$ and $\text{Sc}_i = \mu/(\rho D_i)$, then from (18) the diffusivity coefficient can be computed by:

$$D_i = \frac{\kappa}{\rho C_p \text{Le}_i} . \tag{19}$$

As in this paper we consider air and methane, the assumption of $\text{Le}_i = 1$ is suitable where the thermal and molecular diffusion can be assumed equal for all species [17]. Then, (19) can be simplified to:

$$D = \frac{\kappa}{\rho C_p} . \tag{20}$$

2.3. Fluid properties

The thermochemical properties of air and methane considered in this work are given in Table 1:

Table 1
Fluid properties of methane and air at standard conditions.

Fluid property	Methane	Air
Molecular mass W_i [g/mol]	16.043	28.965
Viscosity μ_i [kg /(m·s)]	$1.1102 \cdot 10^{-5}$	$1.8551 \cdot 10^{-5}$
Heat capacity $C_{p,i}$ [J/(kg·K]	2224.43	1009.39
Thermal conductivity k_i [W/(m·s)]	0.0357	0.0258

2.4. Adjoint method

Within SU2, a discrete adjoint (DA) solver has already been implemented using Algorithmic Differentiation (AD) [21] via the C++ library Code-Differentiation Package CoDiPack [22]. This DA approach is a highly efficient sensitivity methodology that allows for the computation of sensitivities of an objective function such as surface variance, drag, and others at the computational cost that is approximately equal to performing an additional simulation of the primal problem (i.e. the CFD simulation) [12,13]. This enables the use of gradient-based optimization with a large number of design variables. The DA solver has been constructed in a general way, allowing extensions inside SU2 as the one presented in this paper without the need to manually differentiate new variables. Here, we are going to briefly explain the DA approach. First, we can write the following optimization problem:

$$\min_{\alpha} \quad J(V(\alpha), X(\alpha)) \tag{21}$$

$$\text{subject to } V(\alpha) = G(V(\alpha), X(\alpha)) , \tag{22}$$

$$X(\alpha) = M(\alpha) , \tag{23}$$

where $V(\alpha)$ and $X(\alpha)$ are the primitive variables and mesh state as functions of the design variables α, respectively. Likewise, $J(V(\alpha), X(\alpha))$ is the objective function that we aim to minimize. In this paper, it is the variance of the species mass fraction at the outlet. The constraints are the discretized equations $R(V) = 0$ written as a fixed point equation (22) and the mesh state (23), which relates the mesh to the design variables allowing its deformation. This equation (23) is obtained by the solution of the discretized partial differential equation corresponding to the linear elasticity equations in a pseudo-structural mesh deformation approach [23], which we denote by the operator M. Subsequently, we can compute the Lagrangian associated to the optimization problem (21), (22), (23) as follows:

$$L(\alpha, V, X, \Psi, \Phi) = J(V, X) + \Psi^T [G(V, X) - V] + \Phi^T [M(\alpha) - X] , \tag{24}$$

where Ψ and Φ are the so-called adjoint variables of the optimization problem.

It must be noted in (24) that the terms in square brackets represent the optimization constraints. In this way, using the chain rule, we differentiate (24) with respect to the design variables α:

$$\frac{\mathrm{d}L}{\mathrm{d}\alpha}^T = \frac{\partial J}{\partial V}\frac{\partial V}{\partial \alpha} + \frac{\partial J}{\partial X}\frac{\partial X}{\partial \alpha} + \Psi^T\left(\frac{\partial G}{\partial V}\frac{\partial V}{\partial \alpha} + \frac{\partial G}{\partial X}\frac{\partial X}{\partial \alpha} - \frac{\partial V}{\partial \alpha}\right) + \Phi^T\left(\frac{\partial M}{\partial \alpha} - \frac{\partial X}{\partial \alpha}\right). \quad (25)$$

Then, reordering terms, we have:

$$\frac{\mathrm{d}L}{\mathrm{d}\alpha}^T = \Phi^T\frac{\partial M}{\partial \alpha} + \left(\frac{\partial J}{\partial V} + \Psi^T\frac{\partial G}{\partial V} - \Psi^T\right)\frac{\partial V}{\partial \alpha} + \left(\frac{\partial J}{\partial X} + \Psi^T\frac{\partial G}{\partial X} - \Phi^T\right)\frac{\partial X}{\partial \alpha}. \quad (26)$$

As we desire to avoid the expensive computations of Jacobians $\frac{\partial V}{\partial \alpha}$ and $\frac{\partial X}{\partial \alpha}$ in (26), we can choose Ψ and Φ such that the terms in brackets are zero. This leads to the adjoint equations shown below:

$$\Psi^T = \frac{\partial J}{\partial V} + \Psi^T\frac{\partial G}{\partial V}, \quad (27)$$

$$\Phi^T = \frac{\partial J}{\partial X} + \Psi^T\frac{\partial G}{\partial X}. \quad (28)$$

Thus, by solving the fixed point equation (27) and equation (28), we can compute the sensitivities as follows:

$$\frac{\mathrm{d}J}{\mathrm{d}\alpha}^T = \frac{\mathrm{d}L}{\mathrm{d}\alpha}^T = \Phi^T\frac{\partial M}{\partial \alpha}. \quad (29)$$

Finally, the shape design is done using the SciPy SLSQP optimizer [24], where we update the design variable based on the previous design state, and the sensitivity (29):

$$\alpha^{k+1} = f\left(\alpha^k, \frac{\mathrm{d}J}{\mathrm{d}\alpha}^T\right). \quad (30)$$

In summary, the adjoint-design cycle is shown in the following Fig. 2:

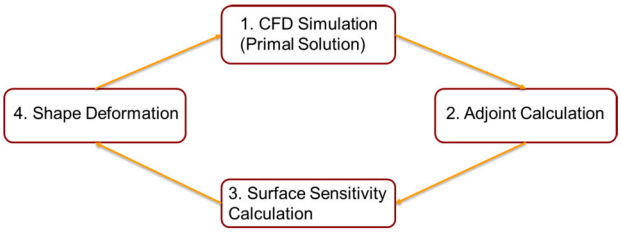


Fig. 2. Adjoint-design cycle.

2.5. Geometry and boundary conditions

The geometry of a Kenics static mixer is defined by the entrance and exit lengths, L_{ent} and L_{exit} respectively, diameter D, blade thickness a and mixer element length L, see Fig. 1. We define the aspect ratio AR as the ratio between the length L of a mixing element and the diameter D:

$$AR = \frac{L}{D}. \quad (31)$$

In the present paper, the diameter is $D = 2$ cm. Based on previous work [7,9–11], in order to study the aspect ratio effects, the following three different aspect ratios are considered: 1.0, 1.5 and 2.0. Similarly, the effect of the blade thickness is analyzed by considering three different blade thicknesses: 1 mm, 2 mm and 3 mm. The entrance length L_{ent} and the exit length L_{exit} are fixed at $4D$ and $6D$, respectively. It must be noted that the entrance and exit sections are used in order to have a fully developed flow at the entrance of the first mixing unit and to prevent backflow at the outlet, respectively. The computational geometry and the structured meshes were generated using Gmsh [25]. The number of elements in the mesh range from 128790 to 383940 elements depending on the aspect ratio studied. Additionally, from Fig. 3, we consider two inlets: a fuel inlet where pure methane is injected ($Y_1 = 1.0$, $Y_2 = 0.0$), and air inlet where pure air is injected ($Y_1 = 0.0$, $Y_2 = 1.0$). Both streams have a temperature of 300 K, and velocity of 5 m/s. The walls are considered isothermal. In this paper, as we are mixing two different gases with the same velocity at each inlet, Re is different. Therefore, the Reynolds number is estimated as the mean value between the Re at each inlet given as follows:

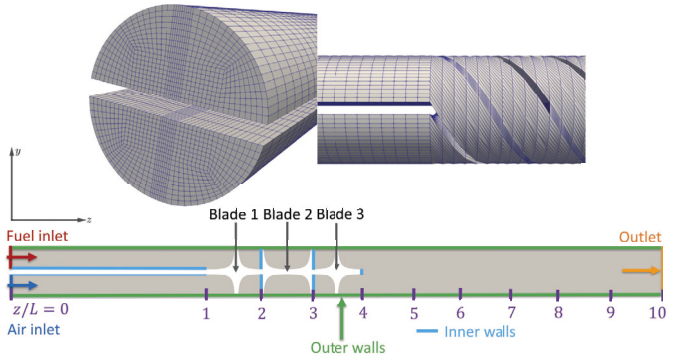


Fig. 3. Computational mesh and boundary conditions. In purple colour it is shown the scaling used for plotting the results in the following section 3.

$$Re = \frac{Re_{\text{inlet fuel}} + Re_{\text{inlet air}}}{2}, \quad (32)$$

where

$$\mathrm{Re}_g = \frac{\rho_g U_g D}{\mu_g}, \quad (33)$$

and ρ_g, U_g and μ_g are the density, velocity magnitude and viscosity of the gas at the corresponding inlet.

In this way, this setup gives an average Reynolds number of $= 6.1 \times 10^3$. At the outlet, zero gauge pressure (ambient pressure) is imposed. Finally, for the SST model, a turbulent intensity of 0.05 and a turbulent-to-laminar viscosity ratio of 10 are considered at each inlet.

3. Results and discussion

3.1. Mixing evaluation

Before proceeding with the CFD simulations, we introduce the statistical measures used for quantifying the mixer performance. For measuring the mixing performance inside the mixer device, there exist several statistical measures proposed in the literature [26]. In the present work, we have adopted the coefficient of variation (CoV), also called *mixing intensity*, used in [10,27]:

$$\mathrm{CoV} = \frac{\sigma}{\overline{Y}}, \quad (34)$$

where $\overline{Y}$ is the mean species mass fraction, and σ is the standard deviation of the species mass fraction. Both quantities are mass flux-weighted average quantities given by:

$$\overline{f^i} = \frac{\iint_S f^i \rho(\mathbf{v}\cdot\hat{n})\mathrm{dS}}{\iint_S \rho(\mathbf{v}\cdot\hat{n})\mathrm{dS}}, \quad (35)$$

where f^i is the i-th moment of the quantity f and S is the surface where the i-th moment is computed. The variance of f can be obtained using

$$\sigma^2 = \overline{f^2} - \left(\overline{f}\right)^2. \quad (36)$$

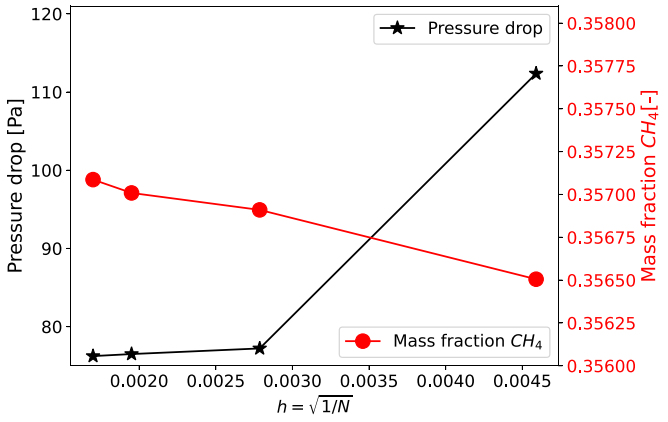


Fig. 4. Pressure drop across the Kenics mixer and mass fraction average of methane at the outlet for 4 different meshes for grid sensitivity analysis. For this simulation, the blade thickness, aspect ratio, and Re are set to $a = 2$ mm, $AR = 1.0$ and $Re = 6.1 \times 10^3$, respectively.

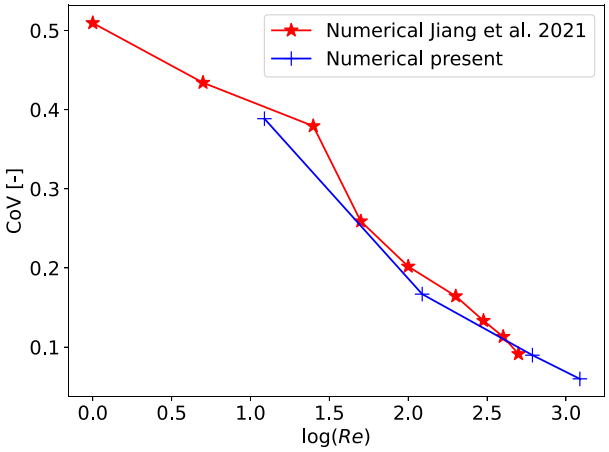


Fig. 5. Comparison of CoV for low Reynolds number with results obtained by [10]. For these simulations $D = 2$ cm, $a = 2$ mm, and $AR = 1.0$.

In our case, $f = Y_1$, the species mass fraction of stream 1. Furthermore, it must be noted that reducing the variance of Y_1 implies a reduction of the variance of Y_2 as well because, as $Y_2 = 1 - Y_1$, then:

$$\sigma_2^2 = \sigma_1^2 . \tag{37}$$

In our analysis, the CoV is being computed simultaneously with the surface total pressure at different cross sections in the mixer, to compare the effect of the geometrical parameters on both quantities.

Furthermore, in order to clearly identify the effects of geometrical parameter changes on the performance of individual blades, we scale the z-axis by the mixer element length L. In this way, when z is between 1 and 4, it means that we are inside the mixing units. Note however that the distance z up to the first mixing unit is scaled by the entrance length L_{ent}, and only from this point onward the z axis is scaled by L, see Fig. 3. Finally, it should be noted that the mixing process occurs starting from the second blade ($z/L = 2$) onward. Therefore, the results regarding CoV are plotted from $z/L = 2$. However, the results regarding pressure drop are plotted along the complete Kenics static mixer starting from $z/L = 0$, considering the inlet section and first mixer unit. This Kenics static mixer configuration was chosen in order to compare the current results with previous works where a similar configuration was used [9–11].

3.2. Grid independence test

To ensure that numerical results are independent of the mesh size, a grid independence test is performed. In this test, four mesh configurations were considered with an increasing number of elements. The number of elements used for the four meshes are 47466, 128790, 262881, and 346356. For each mesh, the pressure drop across the Kenics static mixer and the mass-flux weighted average of the species mass fraction of methane at the outlet are analyzed using (35). From Fig. 4, we can observe that for the coarse mesh with $N = 47466$ cells, the pressure drop and average mass fraction of methane show large differences in comparison to the other mesh configurations. However, for the other three meshes, we can observe that the results are nearly the same. For pressure drop, we observe a change of less than 1.3%. Similarly, for the mass fraction average of methane at the outlet, the results change by less than 0.05%. Hence, based on these results, the mesh of $N = 128790$ elements is chosen for the subsequent simulations when the $AR = 1.0$. Finally, it must be noted that, when $AR = 1.5$ and $AR = 2.0$, the number of elements is increased in order to ensure a high mesh quality within the mixing units.

3.3. Comparison with experimental and simulation data

We compare the results obtained with the data available in the literature. In previous works, such as [5,7,10], the authors considered a single phase liquid with a tracer. Then, the Reynolds numbers were constant at each inlet in those previous works. In this paper, as we are mixing two different gases with the same velocity at each inlet, Re is different. Therefore, the Reynolds number is estimated using (32). Then, we compare the mixing efficiency for low Re with the numerical results obtained by [10]. For these simulations, the velocities considered are 0.01, 0.1, 0.5, 1.0, and 5 m/s. Additionally, the Kenics mixer configuration is $D = 2$ cm, $a = 2$ mm, and $AR = 1.0$. It must be noted that, as $Re < 2300$, the flow regime is laminar, thus the SST model (8), (9) is switched off. From Fig. 5, we can observe that, although the cases studied are not completely the same, the results are aligned and it shows that when the Re number increases, the mixing process is enhanced (lower CoV). This means that more uniform mixtures are obtained, which is expected because increasing the velocity (moving from laminar to turbulent regime) enhances the mixing process.

To compare the effect on pressure drop for a wide range of Re numbers, we compare our results with the experimental data reported by Kumar [9]. For this comparison, we use the same setup used in the aforementioned work, where one inlet is considered. Therefore, as in that case the gas considered is air, we set $Y_0 = 1.0$ as the boundary condition at the inlet. In other words, we simulate pure air with only one component. Additionally, for this set of simulations, we have considered $D = 2.54$ cm, $AR = 1.5$, and $a = 2$ mm, which were used in [9]. This is done in order to get a closer comparison with the experimental results reported in the aforementioned work. Then, the pressure drop per unit of element ($\Delta p/n$) is plotted in Fig. 6 with respect to the Reynolds number. From Fig. 6, we can observe that the results show a similar trend compared to the experimental results obtained in [9]. For $Re \leq 5000$, we can see a good agreement with experimental data. Nevertheless, for higher Re, we can observe that there are some disagreements with the experimental data, in particular when the Re numbers are higher than 10000. These disagreements were also observed for the numerical simulations reported in [9].

Therefore, from the previous simulations, we can conclude that the mixing performance in a Kenics static mixer can be improved by reducing the AR and increasing a. However, this causes an increase in the energy (pressure) needed. Thus, in the next section, we are going to apply the DA approach in order to achieve further improvement on mixing performance with negligible increase on pressure drop.

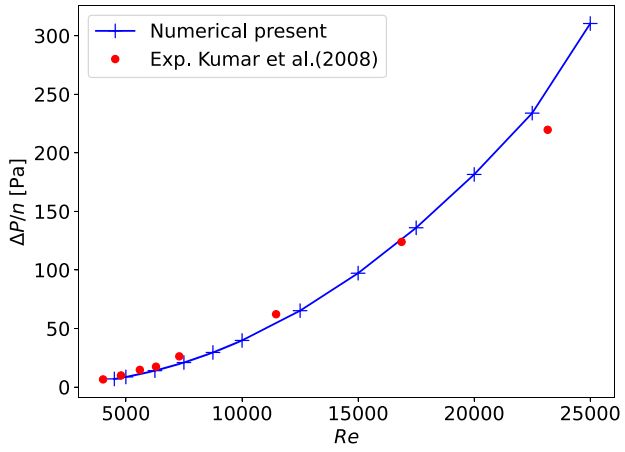


Fig. 6. Comparison of pressure drop per unit element ($n = 3$ in this case) for different Reynolds numbers with the experimental data reported by [9]. For these simulations $D = 0.0254$ m, $AR = 1.5$ and $a = 2$ mm.

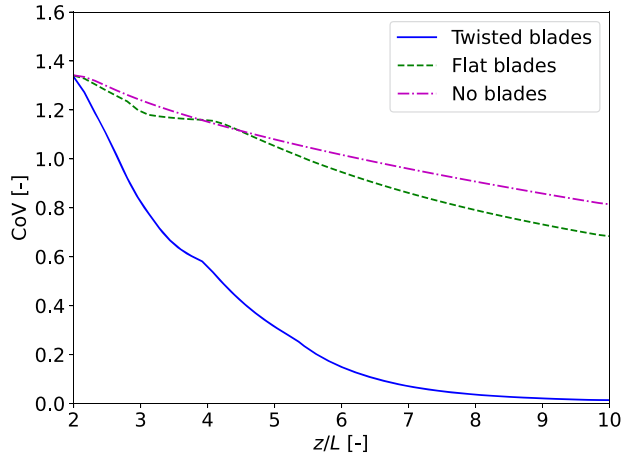


Fig. 7. Comparison of CoV along the Kenics static mixer when no blades (pure diffusion of two gases), twisted and flat blades are considered. For this simulation, we consider $a = 2$ mm, $AR = 1.0$, and $\mathrm{Re} = 6.1 \times 10^3$.

3.4. Effect of blades

First, the effect of the twisted blades inside the Kenics static mixer is compared to a mixer consisting of flat blades. Flat blades consist of straight blades that start perpendicular to the previous one. In this case, the fluid boundary conditions are the ones explained in the previous section 2.5, and the geometrical parameters are $AR = 1.0$ and $a = 1.0$ mm. In Fig. 7, we can observe the mixing performance along the Kenics static mixer when the blades are flat, twisted blades with a rotation angle of 180°, and without blades. It can be observed that twisting the blades enhances the mixing inside the mixing units. This can be explained because twisting the blades forces the flow to be continuously reoriented along the mixing units, increasing velocity gradients, increasing turbulence, which enhances mixing. Conversely, with the flat blades, the flow is not continuously changing, making the mixing process slower. Additionally, the effect of no having blades, in other words, where the two gases diffuse along the empty pipe is shown. We can observe that along the second unit (range 2-3), having flat blades enhances the mixing compared to the case without blades. On the other hand, Fig. 8 shows the effect on the total pressure along the Kenics mixer with twisted and flat blades. We can observe that higher pressure at the inlets is required when the blades are twisted in comparison to the flat blades and the case without blades. This can be explained because as the flow is continuously reoriented, higher pressure is required to keep

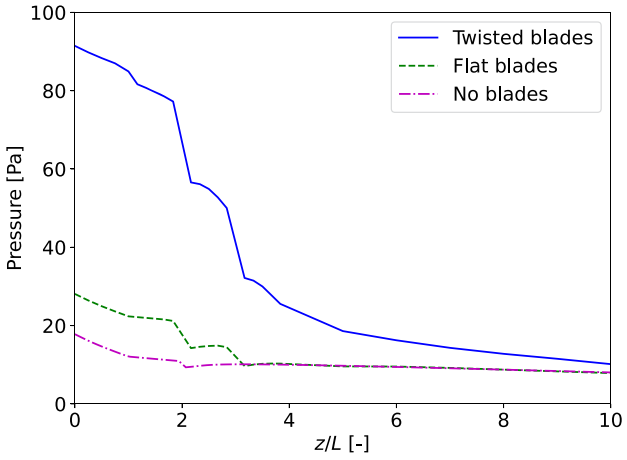


Fig. 8. Comparison of total pressure along the Kenics static mixer when no blades (pure diffusion of two gases), twisted and flat blades are considered. For this simulation, it is set $a = 2$ mm, $AR = 1.0$, and $\mathrm{Re} = 6.1 \times 10^3$.

the flow moving along the mixing units. Additionally, we can observe that in the cases of twisted and flat blades, a large pressure loss occurs at the interface of two mixing units.

Therefore, from the previous two figures, we can corroborate that twisting the blades enhances the mixing process but, at the same time, increases the total pressure drop.

3.5. Velocity and species mass fraction profiles

In order to show the three-dimensional velocity profile along the Kenics static mixer, we show the velocity field at different cross sections in Fig. 9. From this Fig. 9, we can observe certain spatial periodicity in the velocity profile where the flow is continuously reoriented along the axial axis. A similar observation was also found in [6]. Similarly, we plot the species mass fraction of methane at the same locations as we plotted the velocity profile. It must be noted that $Y_1 = 0.0$ (blue colour) represents pure air because $Y_2 = 1 - Y_1 = 1.0$. From Fig. 10, we can observe that in the entrance section and the first unit (first and second top-left figures) methane and air are separated by the blade, and cannot mix. Not having the mixing process in the first unit allows to study the pure effect of the mixing unit in the pressure drop. Moreover, we can observe from position $z/L = 2.335$ how the mixing process is taking place inside the units mixers. It can be seen that twisting the blades enhances the mixing in the second unit (third and fourth top-right figures). Similarly, we can observe that starting the third unit perpendicular to the previous one, increases the mixing process (first and second bottom-left figures). Finally, we can observe a rather uniform mixture in the outlet section (third and fourth bottom-right figures). Therefore, we can conclude that the good performance of the Kenics static mixer is mainly due to the twisted blades and the sharp change between two subsequent units due to the perpendicularity between their blades.

3.6. Effect of blade thickness

The effect of the blade thickness a is evaluated in Figs. 11, 12, and 13 with respect to the mixing performance and total surface pressure along the Kenics static mixer, respectively. From Fig. 11, we can observe that when the blade thickness increases, the CoV decreases. This implies that more uniform mixtures are obtained. This might be explained because as the blade thickness increases, the effective area inside the mixing units decreases, causing an increase in the velocity which enhances the mixing along the mixing device. However, we can also observe from Fig. 12 that increasing the blade thickness from $a = 2$ mm to $a = 3$ mm causes a slight increase (almost negligible) in the mixture uniformity.

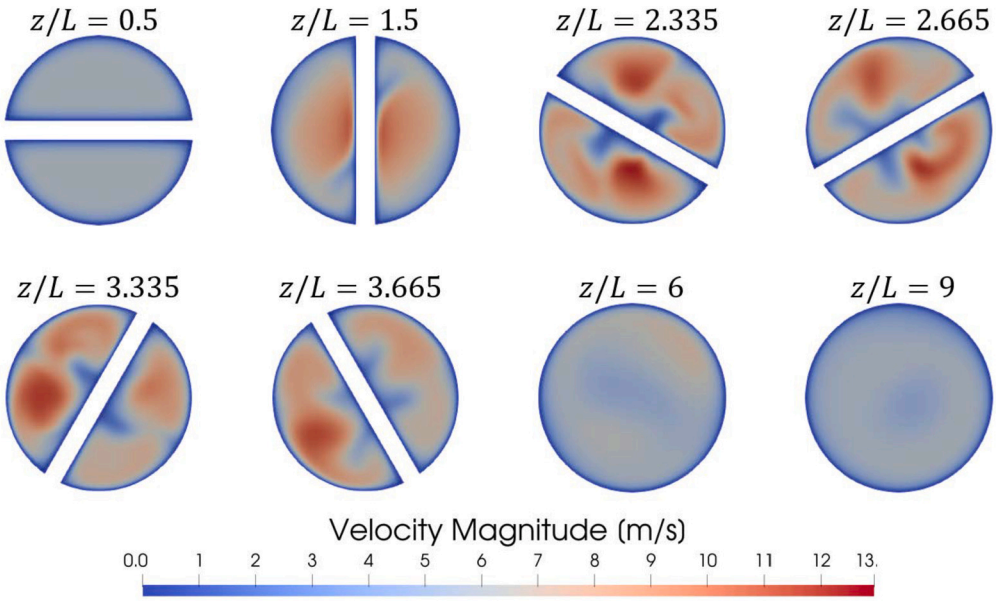


Fig. 9. Velocity magnitude along the Kenics static mixer. The plots are cross sections of the Kenics static mixer device at the locations $z/L = 0.5$, 1.5, 2.3, 2.6, 3.3, 3.6, 6 and 9 (read from top-left to bottom-right). For this simulation, $a = 2$ mm, $AR = 1.0$, and $Re = 6.1 \times 10^3$.

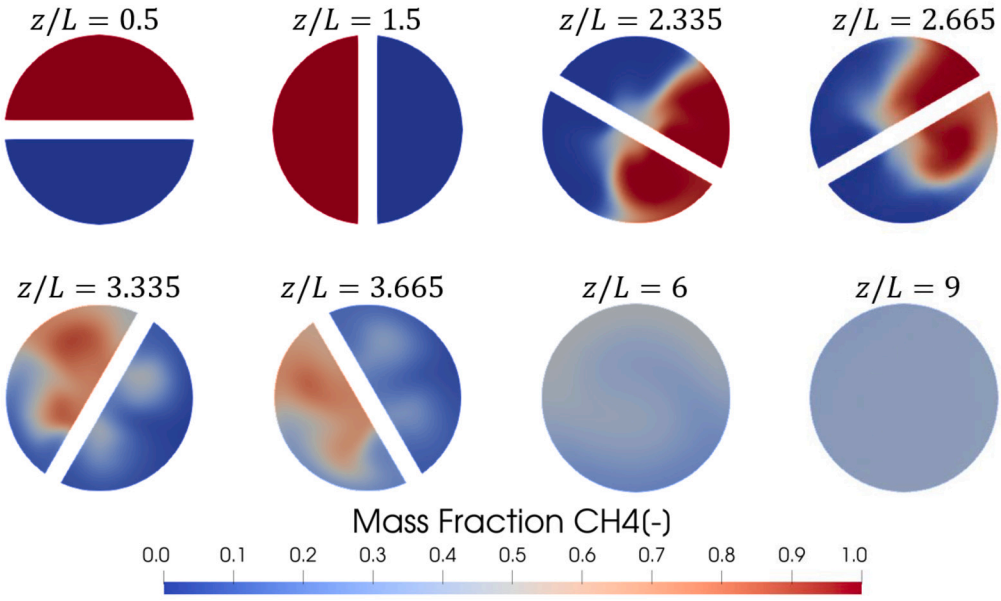


Fig. 10. Mass fraction of methane (Y_1) along the Kenics static mixer. The plots are cross sections of the Kenics static mixer device at the locations $z/L = 0.5$, 1.5, 2.3, 2.6, 3.3, 3.6, 6 and 9 (read from top-left to bottom-right). For this simulation, $a = 2$ mm, $AR = 1.0$, and $Re = 6.1 \times 10^3$.

Therefore, we can conclude that increasing the blade thickness beyond 3 mm might not cause significant changes in the mixing performance.

From Fig. 13, we can observe that the total pressure increases when the blade thickness increases. This might be because by the larger frontal area of the blades, because the pressure drop is larger at the interfaces between the units. Therefore, we can conclude that one way of increase the mixing performance is increasing the blade thickness until a limit is reached (in this case 3 mm). However, this has a cost of increasing the pressure drop along the mixing device. Hence, improving mixing performance and reducing the pressure drop are two goals that compete with each other.

3.7. Effects of the aspect ratio

In Figs. 14, 15, we analyse the effect of the aspect ratio (AR) on the mixing performance and pressure along the Kenics static mixer. It must be noted that the AR is changed by increasing L in (31). From Fig. 14, we can observe that increasing the AR increases the CoV. This means that less uniform mixtures are obtained when the elements are longer. This can be explained because the residence time inside each unit is larger when the AR increases as it was also observed in [10]. Fig. 15 shows that larger pressures are required when the AR decreases. This is because more energy, which is related to the pressure drop, is needed for keeping the flow moving in shorter distances with continuous and sharp changes in the geometry causing flow separation and friction walls, as it is the case inside the Kenics static mixer.

3.8. Adjoint-based design optimization

The results of the parameter study in the previous section are used as a starting point for the adjoint design optimization. We set the aspect ratio equal to 1.0, and the initial blade thickness to 2 mm. The flow

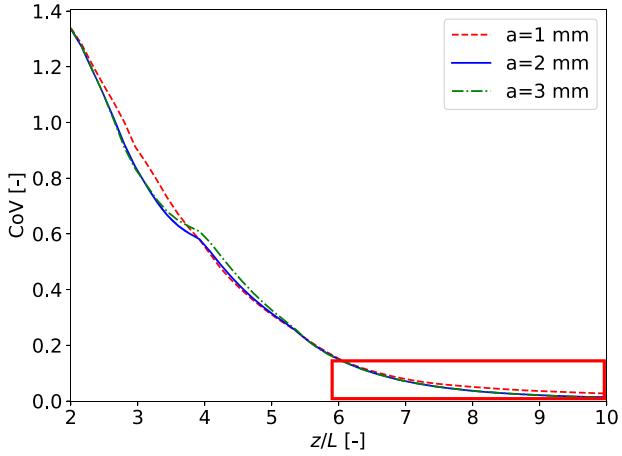


Fig. 11. CoV along the Kenics static mixer for different blade thickness. The red square marked is a zoom of the final zone of the Kenics static mixer plotted in Fig. 12. For these simulations, the aspect ratio (AR) is set to 1.0 and Re = 6.1×10^3.

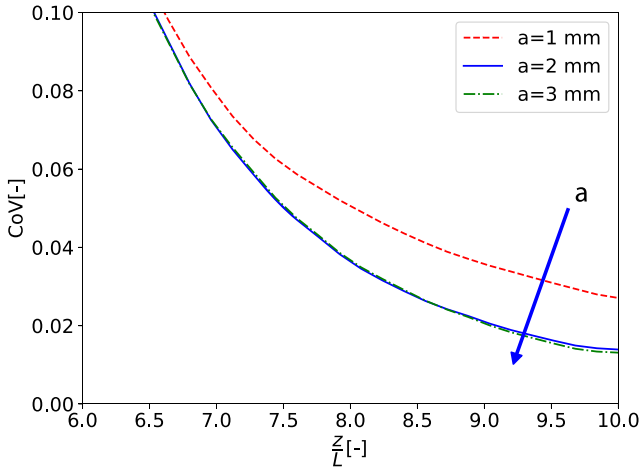


Fig. 12. CoV along the Kenics static mixer for different blade thickness. Zoom of the red square marked in Fig. 11.

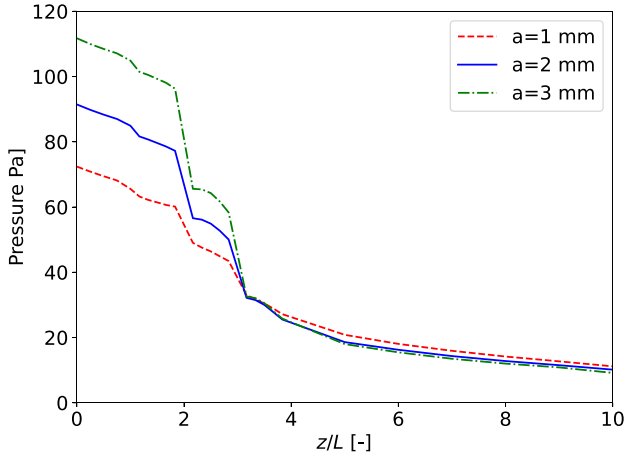


Fig. 13. Pressure along the Kenics static mixer for different blade thickness. For these simulations, the aspect ratio (AR) is set to 1.0 and Re = 6.1×10^3.

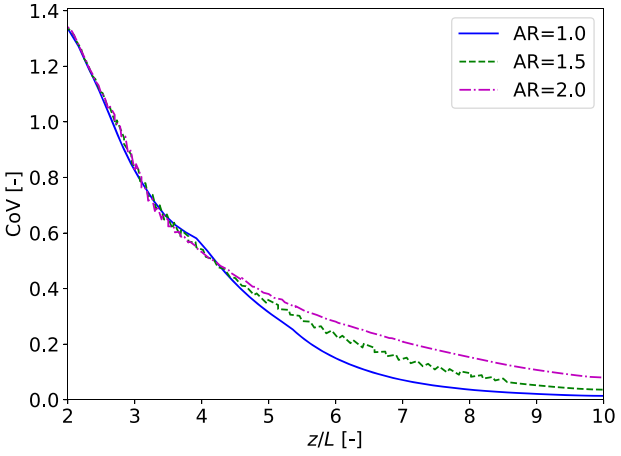


Fig. 14. CoV along the Kenics static mixer for different aspect ratios. For these simulations, the blade thickness (a) is set to 2 mm and Re = 6.1×10^3.

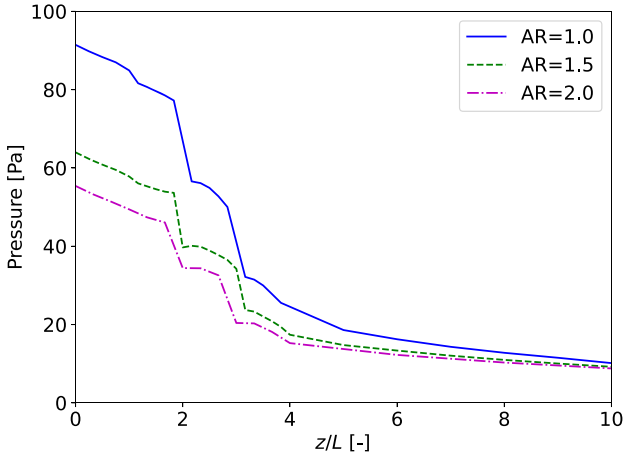


Fig. 15. Pressure along the Kenics static mixer for different aspect ratios. For these simulations, the blade thickness (a) is set to 2 mm and Re = 6.1×10^3.

conditions are the ones explained in section 2.5, where, using (32), the flow can be considered turbulent as we have an estimated $Re = 6.1 \times 10^3$.

During the design optimization, the mesh is not deformed directly, a Free Form Deformation Box (FFD-Box) is used [28] (see Fig. 16), where the mesh nodes are related to the FFD-Box using Bezier hyperpatches. This allows to obtain smooth deformations. Thus, the sensitivities (29) are computed with respect to the FFD-Box nodes and, subsequently, they are projected back to the mesh nodes. Then, we consider two FFD-Boxes as is shown in the Fig. 16.

Fig. 17 shows a cross-section of the FFD-box used. The FFD-Box is constructed in such a way that it is completely inside the Kenics static mixer and its diagonal is equal to D, the diameter of the mixer. The entire intersection of the blades with the outer wall is now just outside of the FFD-box. This setup fixes the blade twist and prevents deformation of the pipe wall. As the mixing between the two streams starts at the intersection between the first and the second mixing unit, we aim to optimize only the shape of the second and third unit. The FFD-box is discretized using an equal number of nodes in the 3 spatial directions. We are considering 6, 11 and 21 nodes per direction (5, 10 and 20 subdivisions of each FFD-Box, respectively). This gives boxes with 128, 1458 and 13718 design variables, respectively. In this way we can investigate the impact of the number of design variables on the performance and the design. As we can observe from Fig. 16, the second blade starts perpendicular to the previous blade in the direction y. Then, for this blade, the deformation is allowed only in the x-direction. Similarly,

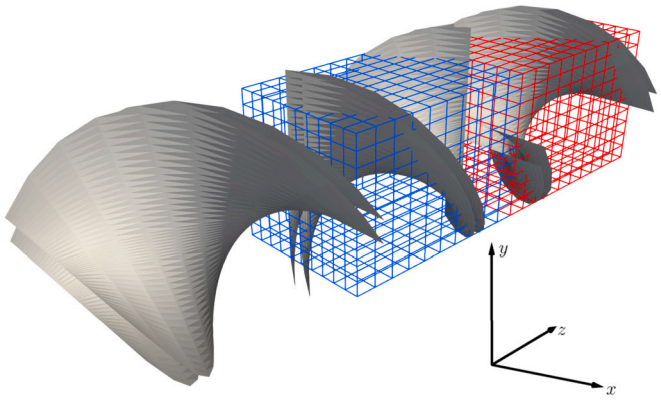


Fig. 16. FFD-Boxes used for blades design optimization. Box for blade 2 in blue, box for blade 3 in red.

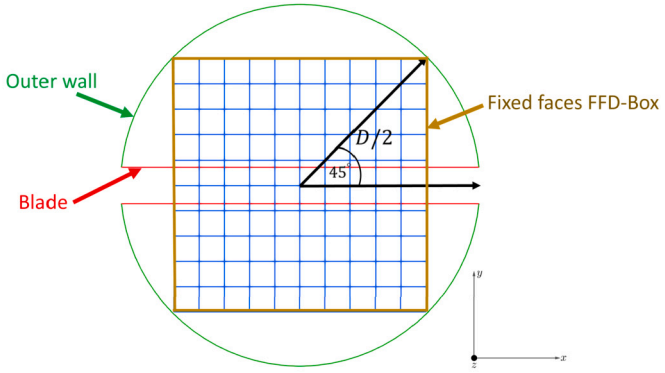


Fig. 17. Schematic representation of the FFD-Box construction used for the DA-design approach.

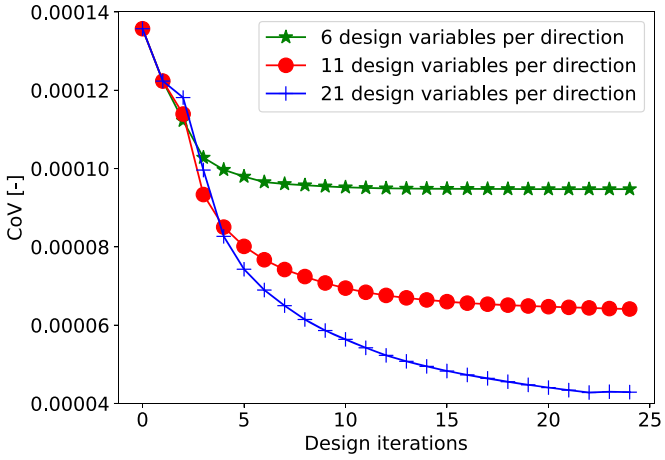


Fig. 18. Convergence of the Coefficient of Variation as a function of the number of design iterations when 6, 11 and 21 design variables per direction are considered.

in the third blade, the deformation is only allowed in the y-direction. Moreover, as the blades intersect the walls of the mixer device, large deformations could cause undesired changes in the outer-structure of the Kenics static mixer. Thus, the deformation in each direction that is going to be deformed is limited to a maximum value. In this case, the maximum is 1 mm, which represents 5% of the diameter.

We perform the adjoint-design cycle considering as the objective function the surface variance of the species mass fraction at the outlet,

$$J(V, X) = \sigma^2_{\text{Outlet}} \,. \tag{38}$$

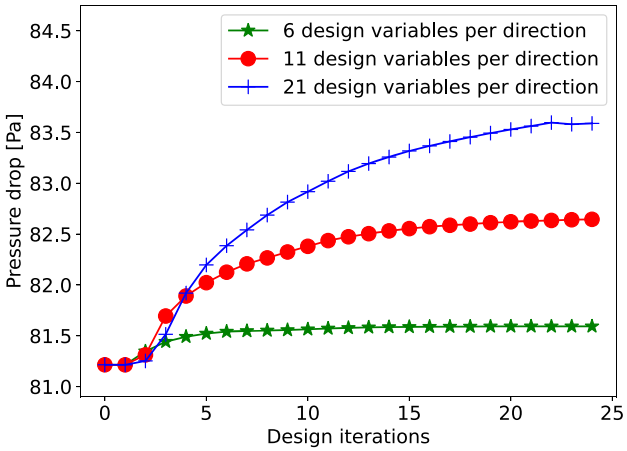


Fig. 19. Pressure drop as a function of the number of design iterations when 6, 11 and 21 design variables per direction are considered.

Table 2
Comparison of pressure drop (ΔP) and coefficient of variation (CoV) between initial and optimized designs for the design variables per direction (α) considered in this work.

α	ΔP [Pa]	CoV [-]
Initial	81.215	$1.357 \cdot 10^{-4}$
6	81.593	$9.474 \cdot 10^{-5}$
11	82.645	$6.412 \cdot 10^{-5}$
21	83.589	$4.289 \cdot 10^{-5}$

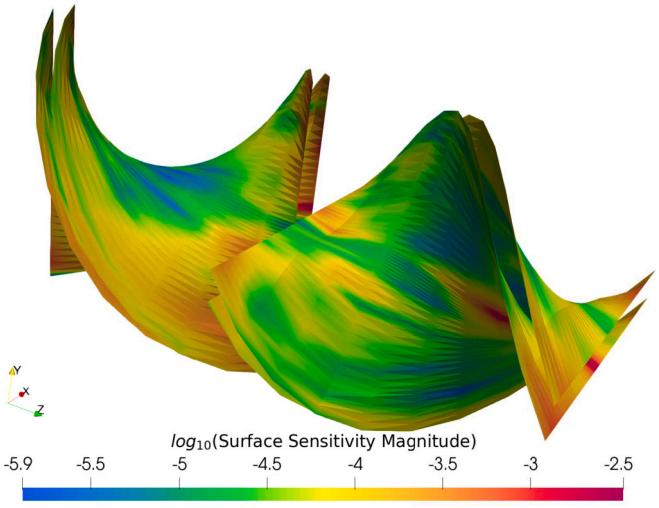


Fig. 20. Surface sensitivity magnitude of the second blade and third blade.

For each design iteration, we can observe the change in the objective function for 6, 11 and 21 design variables per direction ($\alpha = 128, 1458,$ and 13718, respectively) in Fig. 18. Starting from the second iteration, we observe a slightly higher reduction in the objective function when 6 and 11 design variables are considered, compared to the case of 21 design variables. This can be explained because when 6 and 11 design variables are considered, the deformation along the blades might be larger and less smooth in comparison to the cases when 21 design variables are considered. Nevertheless, we can observe that considering more design variables (11 and 21 design variables in this case) provides

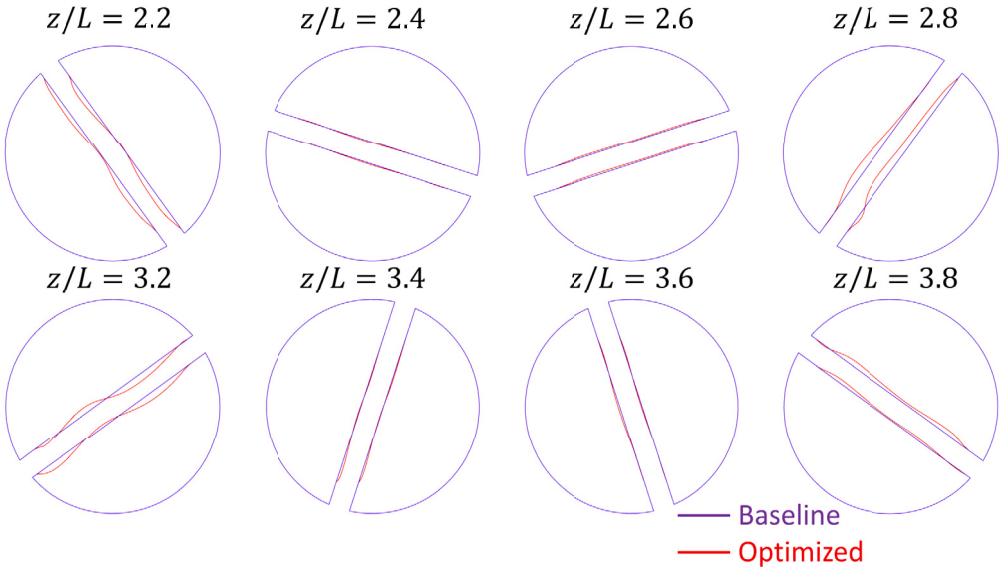


Fig. 21. Baseline and optimized design at different cross sections of the Kenics Static Mixer. Top row corresponds to the second blade. Bottom row corresponds to the third blade.

a larger decrease in the value of the objective function along the adjoint-design cycle, obtaining a reduction in the CoV of around 53% and 68% with respect to the start design, respectively. It can be observed that after 10 design iterations, a minimum is reached in the case of 6 design variables, and no further improvements on the mixing performance are obtained. In this case a reduction of around 30% with respect to the start design is obtained.

We can compute the pressure drop at each design iteration, obtaining the results show in the Fig. 19.

From Fig. 19, we can observe that at the first two design iterations, the pressure drop does not change in the case of 11 and 21 design variables. This has a direct relation with what is observed in Fig. 18, where it is not observed a considerable change in the objective function. As we observed on the previous section, this behaviour is expected because mixing intensity and pressure drop are two quantities that compete each other. This can also be observed when 6 design variables are considered. From the third iteration, we can observe an increase in the pressure drop for both cases. Nonetheless, for 21 design variables, a slight increase is observed. When we compare the start value and the last value, we observe an increase of pressure drop of 0.378 Pa, 1.43 Pa and 2.374 Pa when 6, 11 and 21 design variables per direction are considered, respectively as it is shown in Table 2.

These increases in pressure drop represent a 0.46%, 1.76% and 2.92% increase of pressure drop, respectively, which are almost negligible in comparison to the increase in pressure observed in the previous section when the blade thickness is increased. This relatively small increase might be explained because the blade deformations are smooth, localized and limited to a maximum value.

From Fig. 20 we can observe the surface sensitivities obtained using the DA-design approach. It can be observed that the largest values are localized at the blades corners. This reflects how crucial controlling the deformation at these geometrical constraints is, because, although the DA-design approach is a general and well-formulated mathematical framework, the design of the FFD-Box must be chosen carefully in order to ensure smooth and reasonable geometries for the CFD simulations. Furthermore, from Fig. 21, we can observe different cross sections of the baseline and optimized Kenics mixer design. From this figure, we can observe localized deformations, which are larger at the beginning and end of a mixing element, showing wavy patterns. This might cause accelerations and decelerations of the flow, increasing the recirculation and, consequently enhancing the mixing process, without increasing substantially the pressure drop along the Kenics static mixer.

4. Conclusions

A framework for a discrete adjoint-based design approach has been applied to multi-species simulations using the multiphysics simulation suite SU2. Composition-dependent mixing models for multi-species flows have been implemented and coupled to the existing discrete adjoint framework within SU2. Subsequently, a parameter study was performed, showing that lower AR, higher a, and higher Re led to a reduction in the mixing intensity (better mixing process) but, at the same time, an increase in the pressure drop. This framework can be used to perform automatic design optimization of mixing devices as was done in this work for a Kenics static mixer. In the previous section 3.8, we showed that a large improvement of the mixing performance can be achieved with a negligible increase in pressure drop. The results show a reduction of more than 50% in the variance of the species mass fraction at the outlet when 11 design variables per direction were considered, with an increase in pressure drop of less than 2%. Therefore, the discrete adjoint approach in SU2 has demonstrated to be a viable optimization tool in the optimization of laminar and turbulent mixing devices.

CRediT authorship contribution statement

Cristopher Morales Ubal: Writing – review & editing, Writing – original draft, Methodology, Investigation, Formal analysis. **Nijso Beishuizen:** Writing – review & editing, Writing – original draft, Supervision, Conceptualization. **Lisa Kusch:** Writing – review & editing, Formal analysis. **Jeroen van Oijen:** Writing – review & editing, Supervision, Methodology, Formal analysis.

Declaration of competing interest

The authors declare that they have no known competing financial interests or personal relationships that could have appeared to influence the work reported in this paper.

Data availability

Data will be made available on request.

References

[1] M. Romańczyk, W. Elsner, Effect of cylindrical turbulators on the mixing process in basic Venturi gas mixer using OpenFOAM, MATEC Web Conf. 252 (2019), https://doi.org/10.1051/matecconf/201925204004.

[2] J.P. Valdés, L. Kahouadji, O.K. Matar, Current advances in liquid–liquid mixing in static mixers: a review, Chem. Eng. Res. Des. 177 (2022) 694–731, https://doi.org/10.1016/j.cherd.2021.11.016.

[3] A. Ghanem, T. Lemenand, D. Della Valle, H. Peerhossaini, Static mixers: mechanisms, applications, and characterization methods – a review, Chem. Eng. Res. Des. 92 (2) (2014) 205–228, https://doi.org/10.1016/j.cherd.2013.07.013.

[4] R. Thakur, C. Vial, K. Nigam, E. Nauman, G. Djelveh, Static mixers in the process industries—a review, in: Reaction Engineering: Microstructured Reactors, Chem. Eng. Res. Des. 81 (7) (2003) 787–826, https://doi.org/10.1205/026387603322302968.

[5] D. Hobbs, F. Muzzio, Optimization of a static mixer using dynamical systems techniques, Chem. Eng. Sci. 53 (18) (1998) 3199–3213, https://doi.org/10.1016/S0009-2509(98)00115-8.

[6] D. Hobbs, P. Swanson, F. Muzzio, Numerical characterization of low Reynolds number flow in the Kenics static mixer, Chem. Eng. Sci. 53 (8) (1998) 1565–1584, https://doi.org/10.1016/S0009-2509(97)00132-2.

[7] H.-S. Song, S.P. Han, A general correlation for pressure drop in a Kenics static mixer, Chem. Eng. Sci. 60 (21) (2005) 5696–5704, https://doi.org/10.1016/j.ces.2005.04.084.

[8] P. Joshi, K. Nigam, E. Nauman, The Kenics static mixer: new data and proposed correlations, Chem. Eng. J., Biochem. Eng. J. 59 (3) (1995) 265–271, https://doi.org/10.1016/0923-0467(94)02948-2.

[9] V. Kumar, V. Shirke, K. Nigam, Performance of Kenics static mixer over a wide range of Reynolds number, Chem. Eng. J. 139 (2) (2008) 284–295, https://doi.org/10.1016/j.cej.2007.07.101.

[10] X. Jiang, N. Yang, R. Wang, Effect of aspect ratio on the mixing performance in the Kenics static mixer, Processes 9 (3) (2021), https://doi.org/10.3390/pr9030464.

[11] X. Jiang, Z. Xiao, J. Jiang, X. Yang, R. Wang, Effect of element thickness on the pressure drop in the Kenics static mixer, Chem. Eng. J. 424 (2021) 130399, https://doi.org/10.1016/j.cej.2021.130399.

[12] T. Albring, M. Sagebaum, N.R. Gauger, Efficient aerodynamic design using the discrete adjoint method in SU2, in: 17th AIAA/ISSMO Multidisciplinary Analysis and Optimization Conference, 2016, p. 3518, https://api.semanticscholar.org/CorpusID:124364739.

[13] T.A. Albring, M. Sagebaum, N.R. Gauger, Development of a Consistent Discrete Adjoint Solver in an Evolving Aerodynamic Design Framework, 2015, https://arc.aiaa.org/doi/pdf/10.2514/6.2015-3240.

[14] T.D. Economon, Simulation and adjoint-based design for variable density incompressible flows with heat transfer, in: Multidisciplinary Analysis and Optimization Conference, 2018, https://arc.aiaa.org/doi/pdf/10.2514/6.2018-3111.

[15] A. Kord, J. Capecelatro, A discrete-adjoint framework for optimizing high-fidelity simulations of turbulent reacting flows, Proc. Combust. Inst. (2022), https://doi.org/10.1016/j.proci.2022.06.021.

[16] C.R. Wilke, A viscosity equation for gas mixtures, J. Chem. Phys. 18 (4) (1950) 517–519, https://doi.org/10.1063/1.1747673.

[17] T. Poinsot, D. Veynante, Theoretical and Numerical Combustion, Edwards, 2005, https://books.google.nl/books?id=cqFDkeVABYoC.

[18] F.R. Menter, Two-equation eddy-viscosity turbulence models for engineering applications, AIAA J. 32 (8) (1994) 1598–1605, https://doi.org/10.2514/3.12149.

[19] J.D. Buckmaster, The Mathematics of Combustion, Society for Industrial and Applied Mathematics, 1985.

[20] B. Poling, J. Prausnitz, J. O'Connell, The Properties of Gases and Liquids 5E, McGraw Hill Professional, McGraw-Hill Education, 2000, https://books.google.nl/books?id=9tGclC3ZRX0C.

[21] A. Griewank, A Mathematical View of Automatic Differentiation, Acta Numerica, vol. 12, Cambridge University Press, 2003, pp. 321–398.

[22] M. Sagebaum, T. Albring, N.R. Gauger, High-performance derivative computations using codipack, https://doi.org/10.48550/ARXIV.1709.07229, 2017.

[23] R.P. Dwight, Robust mesh deformation using the linear elasticity equations, https://api.semanticscholar.org/CorpusID:5932023, 2009.

[24] E.D. Jones, T.E. Oliphant, P. Peterson, Scipy: open source scientific tools for python, https://api.semanticscholar.org/CorpusID:215874460, 2001.

[25] C. Geuzaine, J.-F. Remacle, Gmsh: a 3-d finite element mesh generator with built-in pre- and post-processing facilities, Int. J. Numer. Methods Eng. 79 (11) (2009) 1309–1331, https://doi.org/10.1002/nme.2579.

[26] E.L. Paul, V.A. Atiemo-Obeng, S.M. Kresta (Eds.), Handbook of Industrial Mixing, John Wiley & Sons, Ltd., 2003, pp. i–lxi.

[27] M. Haddadi, S. Hosseini, D. Rashtchian, M. Olazar, Comparative analysis of different static mixers performance by cfd technique: an innovative mixer, Chin. J. Chem. Eng. 28 (3) (2020) 672–684, https://doi.org/10.1016/j.cjche.2019.09.004.

[28] T.W. Sederberg, S.R. Parry, Free-form deformation of solid geometric models, SIGGRAPH Comput. Graph. 20 (4) (1986) 151–160, https://doi.org/10.1145/15886.15903.